Effect of Electric Field On Electron Mobility in Sub-100 nm InAlN/GaN High Electron Mobility Transistors

Peng Cui (pcui@sdu.edu.cn)
Shandong University

Yuping Zeng
University of Delaware

Research Article

Keywords: Electron, mobility, heterostructure, polarization, Hamiltonian

Posted Date: December 29th, 2021

DOI: https://doi.org/10.21203/rs.3.rs-1194683/v1

Effect of electric field on electron mobility in sub-100 nm InAlN/GaN high electron mobility transistors

Peng Cui[1,*] & Yuping Zeng[2]

Abstract

Electron mobility is important for electron velocity, transport current, output power, and frequency characteristics. In conventional mobility extraction methods, electron mobility is usually extracted directly from the measured gate capacitance (C_G) and current-voltage characteristics. When device gate length (L_G) scales to sub-100 nm, the determination of C_G becomes more difficult not only for the measure equipment but also the enhanced effect from parasitic capacitance. Here in this paper, the C_G extracted from high-frequency small-signal equipment circuit is used for the InAlN/GaN high electron mobility transistors (HEMTs). Electron mobility of the device with L_G of 60-nm under V_{DS} of 0.1 V and 10 V is extracted using two-dimensional scattering theory, respectively. The obtained results show that under a high electric field, the electron temperature (T_e) and addition polarization charges ($\Delta\sigma$) increase, resulting in the enhanced polar optical phonon (POP) as well as polarization Coulomb field (PCF) scatterings and degradation of the electron mobility. This study makes it possible to improve the electron mobility by reducing T_e and $\Delta\sigma$ for the InAlN/GaN HEMTs application.AlGaN/GaN heterostructure field-effect transistors with different gate lengths were fabricated. Based on the chosen of the Hamiltonian of the system and the additional polarization charges, two methods to calculate PCF scattering by the scattering theory were presented. By comparing the measured and calculated source-

drain resistances, the influence of the different gate lengths on the PCF scattering potential was confirmed.

[1] Institute of Novel Semiconductors, Shandong University, Jinan, Shandong, 250100, China. [2] Department of Electrical and Computer Engineering, University of Delaware, Newark, DE, 19716, USA. Correspondence and requests for materials

should be addressed to P.C. (email: pcui@sdu.edu.cn).

Introduction

GaN-based high-electron-mobility transistors (HEMTs) indicate great potential for millimeter-wave power applications[1-5]. Electron mobility plays an important role in electron velocity, high-frequency, and output power in GaN HEMTs[6-9]. As we know, many works on electron mobility and carrier scattering model have been reported[10-14]. Polar optical phonon (POP) and polarization Coulomb field (PCF) scattering have been demonstrated as the main scattering mechanisms in GaN HEMTs[10,14,15] . Electron density (n_{2D}) and electron temperature (T_e) dominate POP scattering[10,14]. Addition polarization charges ($\Delta\sigma$) and device dimension (gate length L_G, source-drain spacing L_{SD}, *et al.*) present significant influence on PCF scattering[12,15,16]. In conventional mobility study, the devices with micrometer gate length are usually used[8,17,18]. As devices scale down, the electric field in the channel will increase. The channel electrons can accurate under a high electric field and then T_e increases. Scaling down also changed the device dimension and the effect of $\Delta\sigma$ on small device dimension becomes more significant. Hence, POP and PCF scatterings will be changed with the electric field and device scaling down. But to the best of our knowledge, there are few reports about it. Therefore, extract and study the electron mobility in GaN HEMTs with nanometer L_G is meaningful.

In general, the electron mobility extraction is based on the directly measured gate capacitance (C_G) and current-voltage characteristic[8,17,18]. As devices scale down, the accurate capacitance of small L_G, especially nanometer L_G, is difficult to obtained by directly measurement. In this paper, high-frequency small-signal equipment circuit are used for the C_G extraction. The electron mobility of the InAlN/GaN HEMTs with L_G of 60 nm under drain-source (V_{DS}) of 0.1 V and 10 V is extracted with two-dimensional scattering theory. The obtained results show that under high electric field, the increased

T_e and $\Delta\sigma$ enhance POP and PCF scatterings, resulting in degradation of electron mobility. This makes it possible to further improve device performance for the InAlN/GaN HEMTs application.

Results and discussion

A. Low-Field Electron Mobility

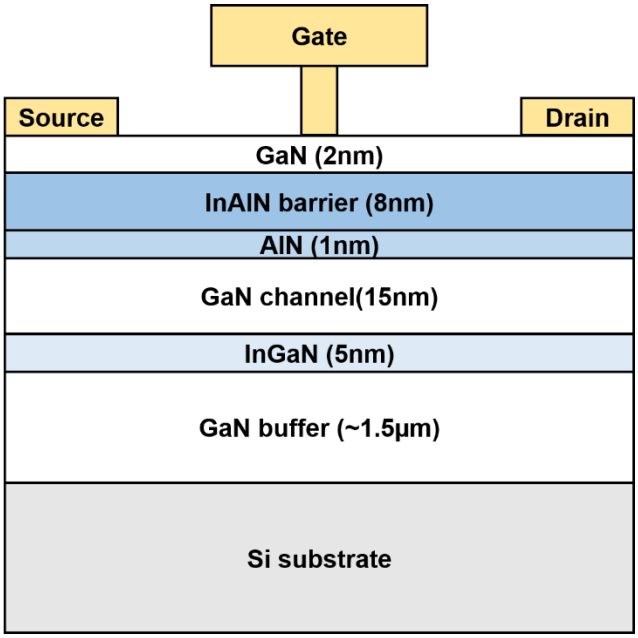

Figure 1. Schematic of the fabricated InAlN/GaN HEMT on Si substrate.

Figure 1 shows the schematic of the fabricated InAlN/GaN HEMT on Si substrate. Devices with source-drain distance (L_{SD}) of 2 μm, gate length (L_G) of 60 ~ 150 nm, and gate width (W_g) of 20 × 2 μm were fabricated. To extract electron mobility, the determination of the electron density (n_{2D}) is very important. In conventional mobility extraction methods, n_{2D} is usually extracted directly from the measured gate capacitance (C_G) of the device with a micrometer gate[8,17,18]. For the devices with sub-100 nm L_G, not only the small gate length requires higher accuracy on the capacitance measurement equipment, the effect from the gate parasitic capacitance (C_{Gext}) on the nanometer gate cannot be ignored[19-21]. The T-shape gate with a larger gate head also increases C_{Gext}, as

shown in **Figure 2** [19-21]. Therefore, the extraction of n_{2D} from the directly measured gate capacitance is not applicable for the sub-100 nm devices.

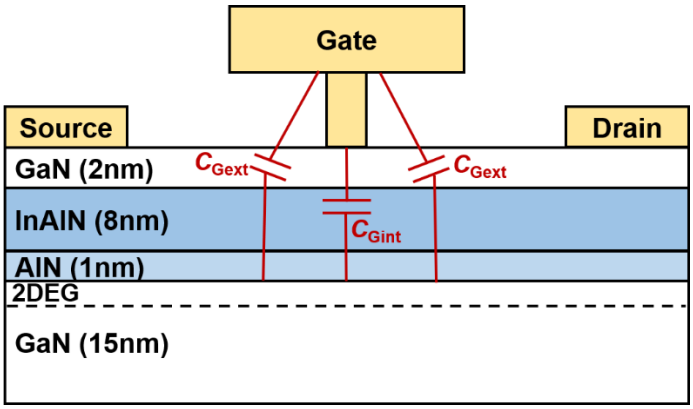

Figure 2. Schematic of C_{Gint} and C_{Gext} under the gate region in InAlN/GaN HEMT.

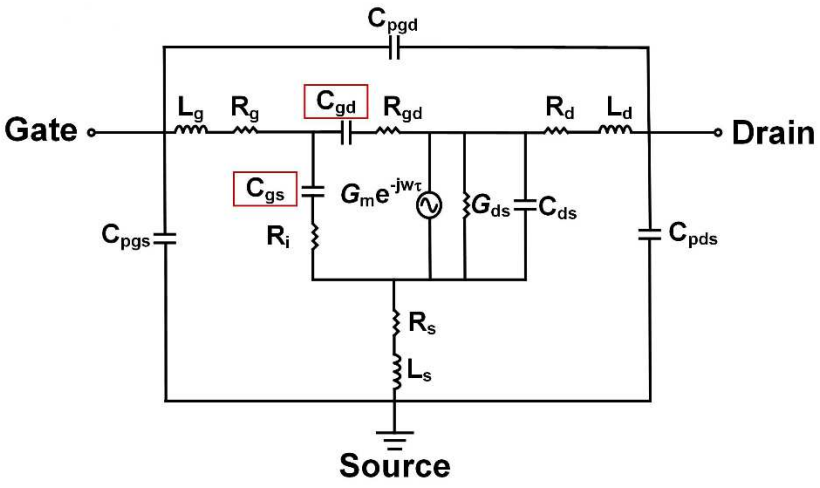

Figure 3. Classical 16-element equivalent-circuit model for InAlN/GaN HEMT.

Another possible method to obtained C_G is from high-frequency *S*-parameters. **Figure 3** shows the classical 16-element equivalent-circuit model for InAlN/GaN HEMTs[22,23]. In the model, C_G is divided into the gate-drain capacitance (C_{GS}) and gate-source capacitance (C_{GS}), which can be obtained from the measured high-frequency S-parameter[22,23].

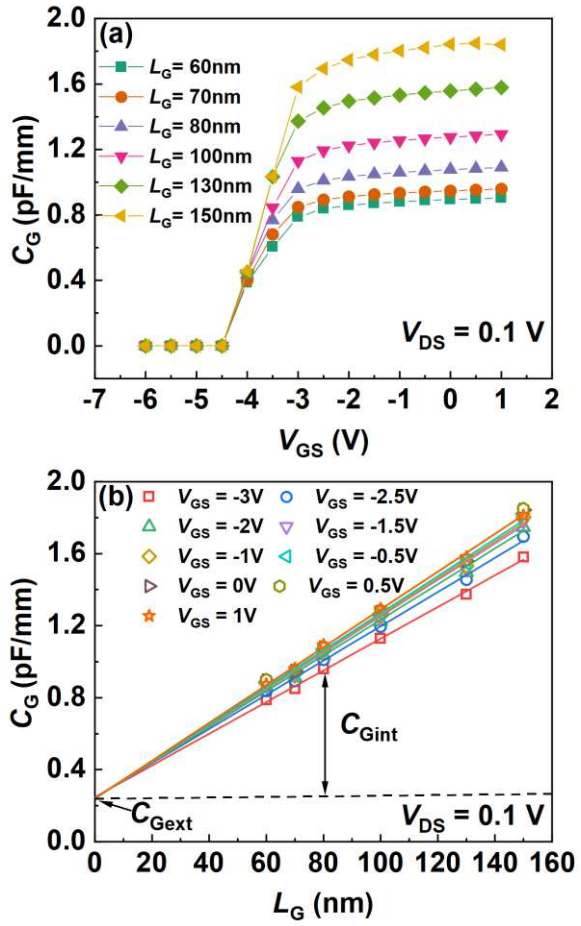

Figure 4. (a) C_G as a function of V_{GS} at V_{DS} = 0.1 V for the InAlN/GaN HEMTs with L_G of 60, 70, 80, 100, 130, 150 nm, respectively. **(b)** C_G as a function of L_G under different V_{GS}. Scatters are the measured results and lines are the fitting curves.

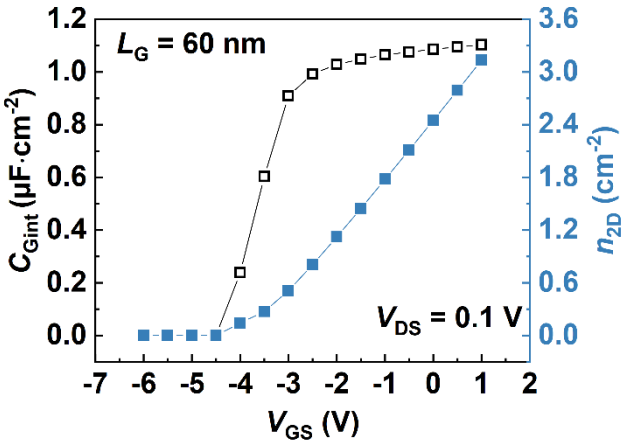

Figure 5. C_{Gint} (left) and n_{2D} (right) as a function of V_{GS} at V_{DS} = 0.1 V for the InAlN/GaN HEMT with L_G = 60 nm.

In this study, the device *S*-parameter is measured from 1 to 50 GHz using an Anritsu MS4647B vector network analyzer. The gate-source voltage (V_{GS}) is changed from -6 to 1 V with 0.5 V step and the drain-source voltage (V_{DS}) is fixed at 0.1 V. With the measured *S*-parameters, C_{GS} and C_{GD} as a function of V_{GS} can be obtained with the classical 16-element equivalent-circuit model**.** Then C_G ($C_G = C_{GS} + C_{GD}$) as a function of V_{GS} under V_{ds} = 0.1 V can be plotted, as shown in **Figure 4(a)**. Here the C_G of the InAlN/GaN HEMTs with L_G of 60, 70, 80, 100, 130, 150 nm are obtained. **Figure 4(b)** shows C_G as a function of L_G under different V_{GS}. Scatters are the measured results and lines are the fitting curves. The measured C_G is linearly dependent upon L_G, in which the Y-intercept corresponds to the C_{Gext}. By subtracting C_{Gext}, the intrinsic gate capacitance (C_{Gint}) can be obtained. **Figure 5** shows a typical result of C_{Gint} versus V_{GS} for the InAlN/GaN HEMTs with L_G = 60 nm. Integrating C_{Gint} with V_{GS}, n_{2D} as a function of V_{GS} is obtained and depicted in **Figure 5**.

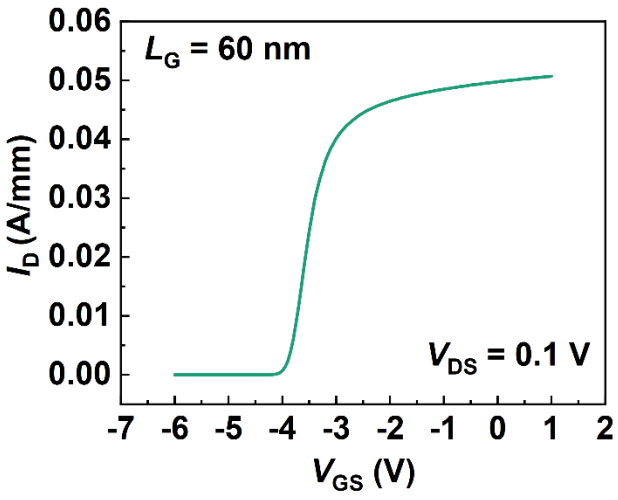

Figure 6. Transfer characteristic at V_{DS} = 0.1 V for the InAlN/GaN HEMT with L_G = 60 nm.

Figure 6 shows the measured transfer characteristic of the InAlN/GaN HEMTs with L_G = 60 nm under V_{ds} = 0.1 V. The total resistance (R) can be extracted from the transfer characteristic, which includes the source-drain material resistance (R_{SD}) and source/drain ohmic contact resistance (R_C). The 2DEG electrons under the gate region is modulated with the gate voltage, but that of the non-gate region (access region) is unchanged. Therefor R_{SD} can be written as[15,24]

$$R_{SD} = R_G + R_{access} = \frac{L_G}{n_{2D} q W_G \mu_G} + \frac{L_{GS} + L_{GD}}{n_{2D0} q W_G \mu_{access}}. \qquad (1)$$

Here R_G and R_{access} are the resistances under the gate region and under the access region, respectively. L_{GS} and L_{GD} are the gate-source and gate-drain distances, respectively. q is the electron charge. n_{2D} is the electron density under the gate region, as shown in **Figure 5**. n_{2D0} is the electron density under the access region, which is the same with the electron density under the gate region at V_{GS} = 0 V. μ_G and μ_{access} are the electron mobility under the gate region and under the access region, respectively.

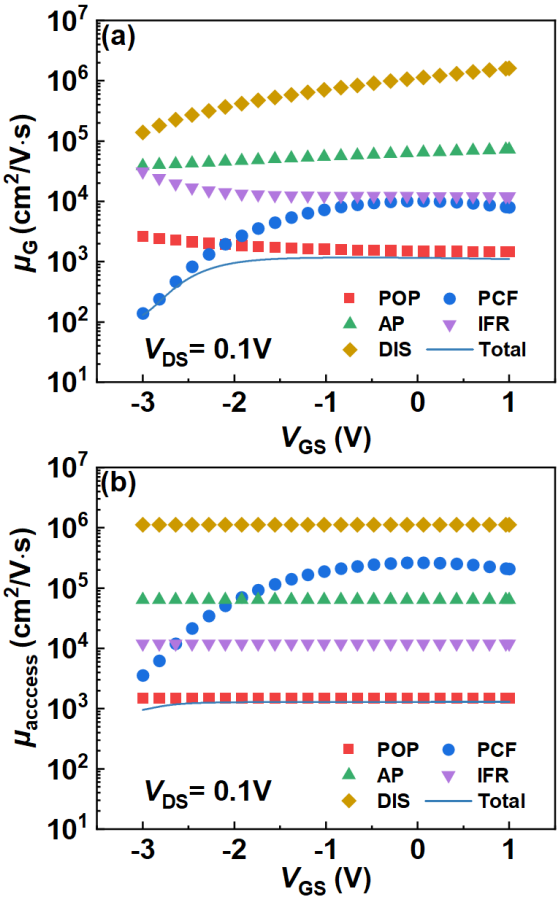

Figure 7. (a) Electron mobility under the gate region (μ_G) limited by different scattering mechanisms as a function of V_{GS} at V_{DS} = 0.1 V. **(b)** Electron mobility under the access region (μ_{access}) limited by different scattering mechanisms as a function of V_{GS} at V_{DS} = 0.1 V.

In InAlN/GaN HEMTs, the main scattering mechanisms include polar optical phonon (POP), polarization Coulomb field (PCF), acoustic phonon (AP), interface roughness (IFR), and dislocation (DIS) scatterings[10,14,15]. Therefore, μ can be obtained from

$$\frac{1}{\mu}=\frac{1}{\mu_{POP}}+\frac{1}{\mu_{PCF}}+\frac{1}{\mu_{AP}}+\frac{1}{\mu_{IFR}}+\frac{1}{\mu_{DIS}}. \qquad (2)$$

Here μ_{POP}, μ_{PCF}, μ_{AP}, μ_{IFR}, and μ_{DIS} are the electron mobility limited by POP, PCF, AP, IFR, and DIS scatterings, respectively, which can be obtained by using two-dimensional scattering theory[10,15]. Hence μ_G and μ_{access} can be determined and is shown

in **Figure 7**. It is significant that POP and PCF scatterings demonstrate the electron mobility. POP scattering is relevant with n_{2D} and electron temperature (T_e). Both increase can enlarge the collision probability between the carriers and lattice atoms, resulting in enhanced POP scatting[10,14]. Here V_{DS} = 0.1 V, channel electric field is very low. T_e is at the temperature and is unchanged. n_{2D} is the only factor that affects POP scatting. Under the gate region, n_{2D} increases with V_{GS} and enhances the POP scatting. PCF scattering comes from the non-uniform of the polarization charges in the InAlN barrier[12,25]. Due to the converse piezoelectric effect, the applied gate voltage can change the polarization charges of the InAlN barrier under the gate region and causes the addition polarization charges ($\Delta\sigma$)[16,26]. $\Delta\sigma$ can cause the PCF scattering potential and result in PCF scattering. Here a more negative V_{GS} causes more $\Delta\sigma$ under the gate region, and leads to larger PCF scatting. Therefore, PCF scattering is enhanced when V_{GS} is shifted to more negative. It can be seen that at V_{GS} < -2 V, PCF scattering demonstrates the total electron mobility. With V_{GS} increases to more than -2 V, the increased n_{2D} causes that POP scattering plays a lead role on electron mobility. Then the total μ_G presents a tread that it increases to a peak and then decreases with the increase of V_{GS}.

Under the access region, the electron density is unchanged with V_{GS}. Therefore, POP, AP, IFR, DIS scatterings are not affected with V_{GS}. As the gate voltage increases, $\Delta\sigma$ decreases and PCF scattering is weakened. Because L_G is 60 nm and L_{SD} = 2 μm, the effect of $\Delta\sigma$ under the small gate region on the large access region is weak, causing PCF scatting of μ_{access} is weaker than that of μ_G.

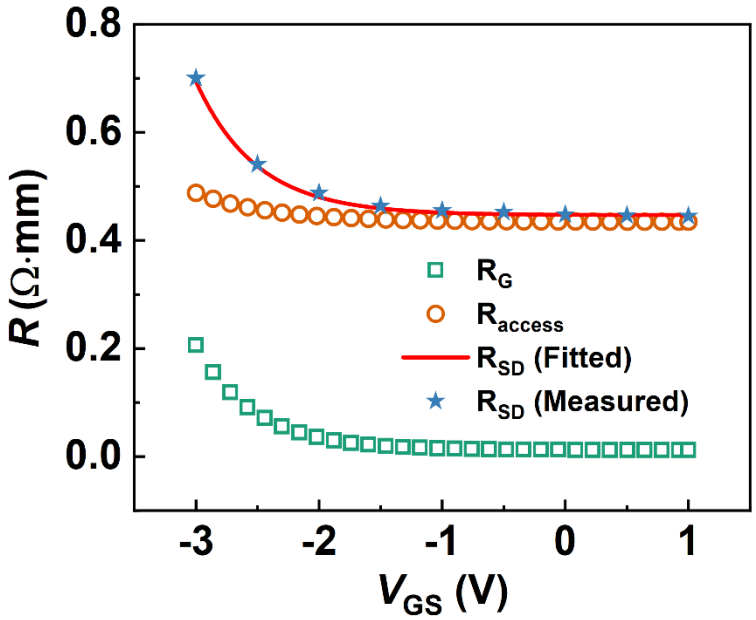

Figure 8. Calculated R_G, R_{access}, calculated R_{SD} (line), and measured R_{SD} (scatters) as a function of V_{GS}.

Based on the extracted μ_G and μ_{access} in **Figure7**, R_G, R_{access} and R_{SD} can be calculated by using (1), as plotted in **Figure 8**. The measured R_{SD} is extracted from transfer characteristic in **Figure 6**. It is shown that the calculated and measured R_{SD} present a good consistence, confirming the accurate of the two-dimensional electron system scattering theory.

B. High-Field Electron Mobility

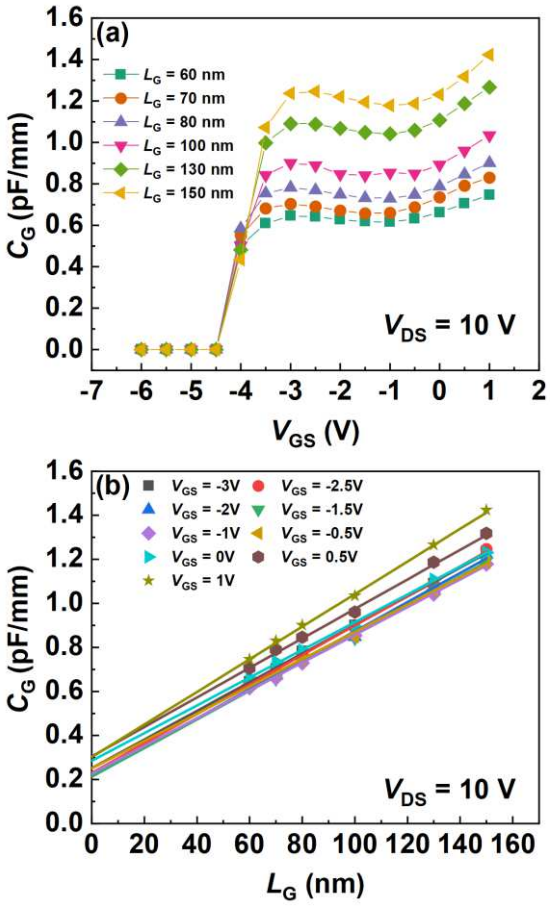

Figure 9. (a) C_G as a function of V_{GS} at V_{DS} = 10 V for the InAlN/GaN HEMTs with L_G of 60, 70, 80, 100, 130, 150 nm, respectively. **(b)** C_G as a function of L_G under different V_{GS}. Scatters are the measured results and lines are the fitting curves.

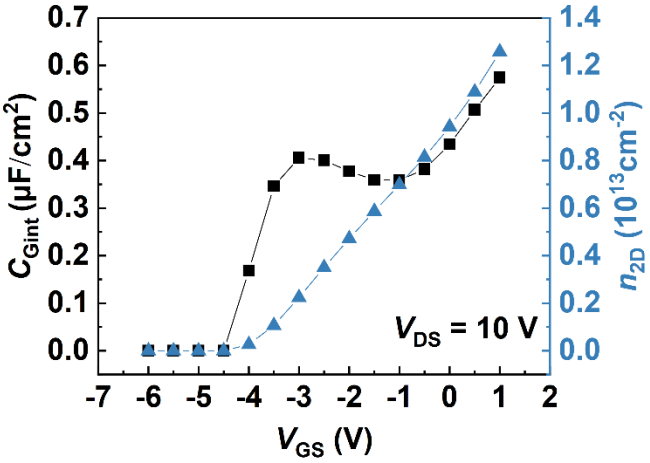

Figure 10. C_{Gint} (left) and n_{2D} (right) as a function of V_{GS} at V_{DS} = 10 V for the InAlN/GaN HEMT with L_G = 60 nm.

The *S*-parameter with frequency of 1 to 50 GHz at V_{DS} = 10 V are also measured. **Figure 9(a)** shows the extracted C_G as a function of V_{GS} at V_{DS} = 10 V for the InAlN/GaN HEMTs with L_G of 60, 70, 80, 100, 130, 150 nm. **Figure 9 (b)** depicts C_G versus L_G under different V_{GS}. A linear dependence of C_G upon L_G is also observed under different V_{GS}. C_{Gext} is obtained from the Y-intercept of the linear fitting curve. Then by subtracting C_{Gext}, C_{Gint} as a function of V_{GS} is plotted in **Figure 10**. n_{2D} is calculated with integration of C_{gint} with V_{GS}. This is also shown in **Figure 10** (see right Y-axis).

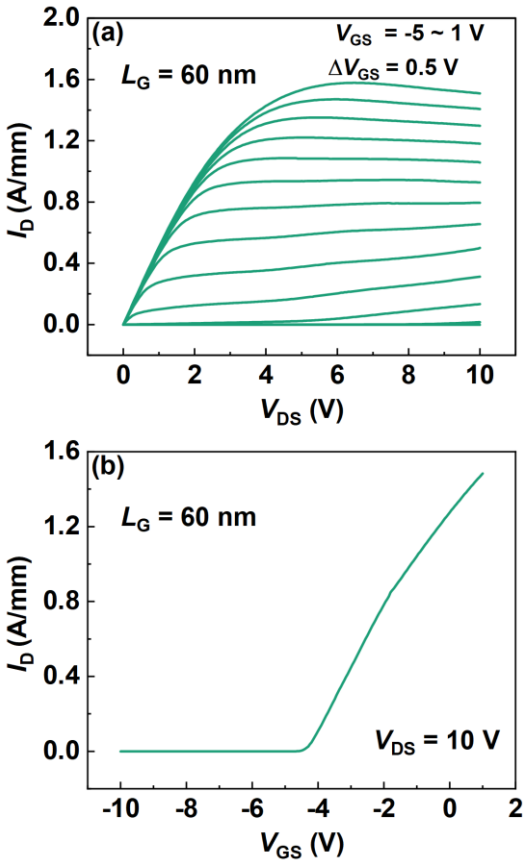

Figure 11. (a) Output and **(b)** transfer characteristics at V_{DS} = 10 V for the InAlN/GaN HEMTs with L_G = 60 nm.

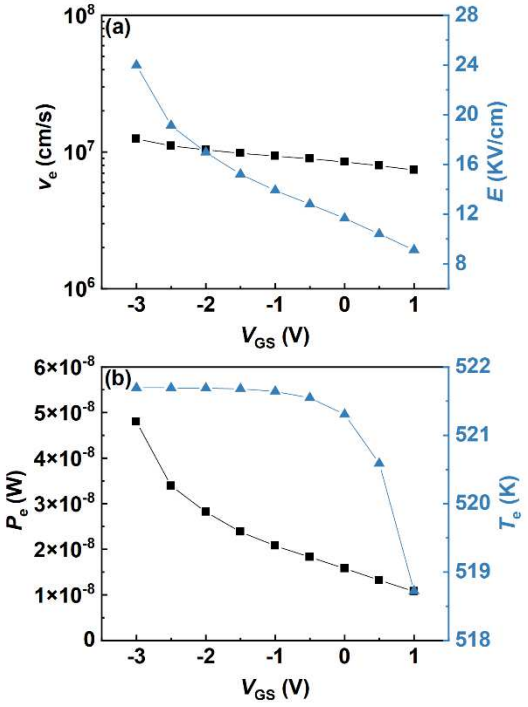

Figure 12. (a) v_e (left) and E (right) as a function of V_{GS}. **(b)** UI/N_e (left) and T_e (right) as a function of V_{GS}.

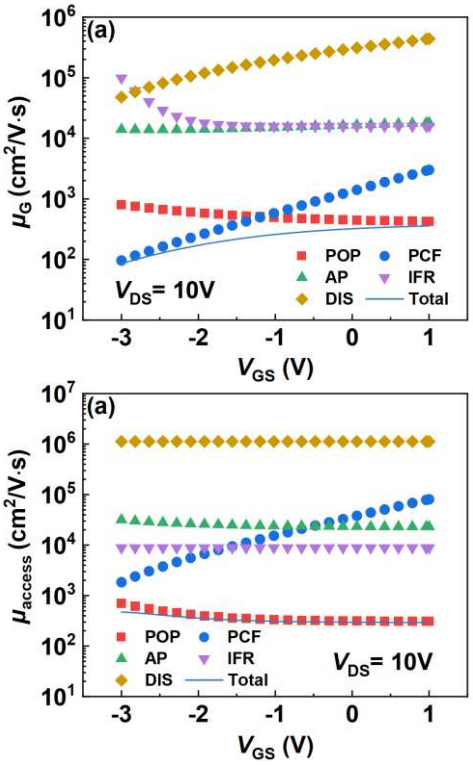

Figure 13. (a) Electron mobility under the gate region (μ_G) limited by different scattering mechanisms as a function of V_{GS} at V_{DS} = 10 V. **(b)** Electron mobility under the access region (μ_{accsee}) limited by different scattering mechanisms as a function of V_{GS} at V_{DS} = 10 V.

Figure 11(a) shows the output characteristic of the InAlN/GaN HEMT with L_G = 60 nm. At V_{DS} = 10 V, the device operates at current saturation region. For the InAlN/GaN HEMT with L_G = 60 nm, the output current saturation is due to the electron velocity (v_e) saturation. In this condition, because the drain-source is very high (V_{DS} = 10 V) and L_{SD} is 2 μm, the electric field in the drain-source channel, especially in the gate channel region is very high. The high electric field can accurate the electrons to high v_e. The electrons with high v_e own a high electron temperature (T_e), which presents significant influence on electron transport[27,28]. **Figure 11(b)** plots the measured transfer characteristic at V_{DS} = 10 V of the same device. With the obtained n_{2D} in **Figure 10** and the drain current I_D in **Figure 11(b)**, v_e is obtained from $I_D = n_{2D}qv_e$. Based on the dependence of v_e on electric field (E) in GaN HEMTs, E can be determined [27]. **Figure 12** depicts v_e and E in the gate channel region as a function of V_{GS}. When V_{GS} increases from -3.5 V to 1 V, v_e decreases from 1.24×10^7 cm/s to 7.38×10^6 cm/s, and E decreases from 23.99 kV/cm to 9.12 kV/cm. The supplied power per electron $P_e = EI_D/n_{2D}$ is calculated with the obtained E. Based on the relationship between T_e and P_e, T_e can be determined[27,28]. **Figure 13** presents P_e and T_e as a function of V_{GS}. As V_{GS} increases, P_e decreases from 4.79×10^{-8} W to 1.08×10^{-8} W, and T_e decreases from 521.7 K to 518.7 K. At V_{DS} = 0.1 V, because the low electric field, electron temperature is at the room temperature (T_e = 300 K). Compared with V_{ds} = 0.1 V, T_e increases from 300 K to ~ 520 K, resulting in an 73% increase of T_e.

With the obtained n_{2D} and T_e, the electron mobility at V_{DS} = 10 V can be calculated by using 2D scattering theory. **Figure 13** shows the calculated μ_G and μ_{access} at V_{DS} = 10 V. POP and PCF scatterings are still the main scattering mechanisms at V_{DS} = 10 V, which is the same with that at V_{DS} = 0.1 V. Compared with the electron mobility at V_{DS} = 0.1 V, μ_{access} presents a slight decrease, but μ_G shows a large decrease. The influence

of electric field on the electron mobility is discussed in the following part.

C. Influence Electric Field on Electron Mobility

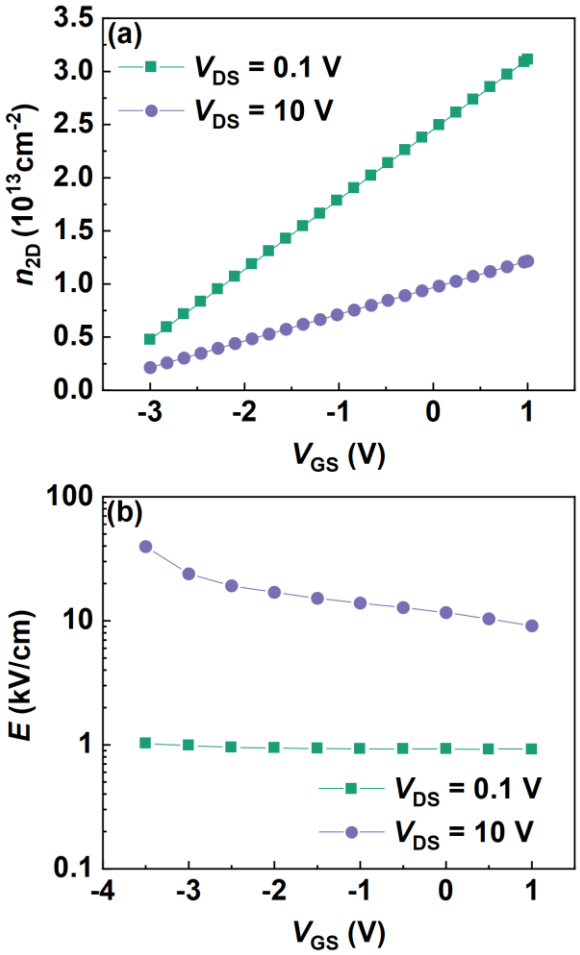

Figure 14. (a) n_{2D} and **(b)** E as function of V_{GS} under V_{DS} of 0.1 and 10 V.

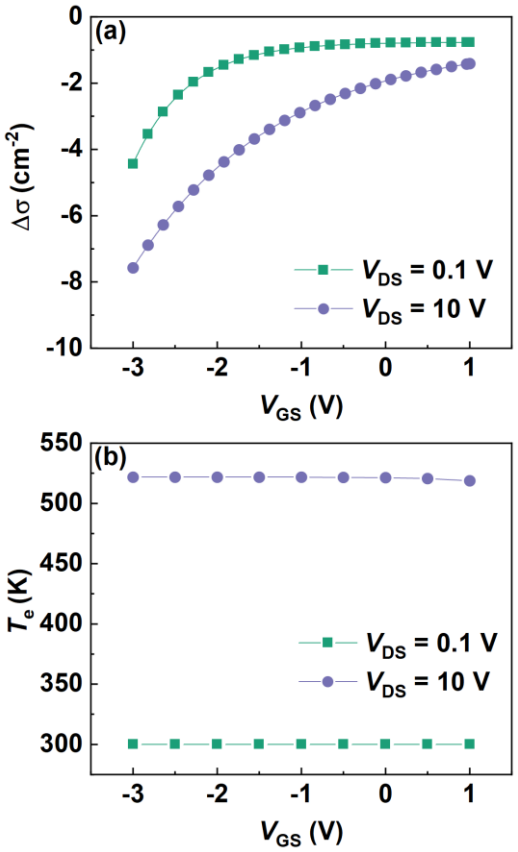

Figure 15. (a) $\Delta\sigma$ and **(b)** T_e as function of V_{GS} under V_{DS} of 0.1 and 10 V.

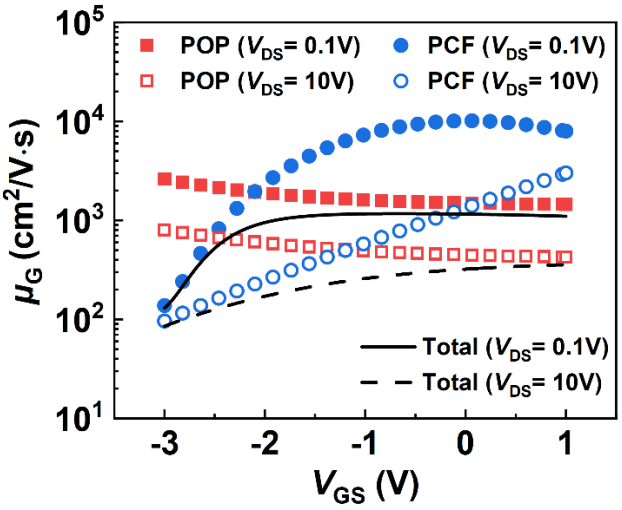

Figure 16. Electron mobility under the gate region (μ_G) limited by POP (POP), PCF scatterings (PCF) and total μ_G (Total) as a function of V_{GS} under V_{DS} of 0.1 and 10 V, respectively.

Figure14(a) compares the n_{2D} at V_{DS} = 0.1 V and 10 V. At high V_{DS}, n_{2D} presents a significant decrease, which results from the improved channel electric potential. **Figure 14(b)** depicts the channel electric field as a function of V_{GS} and more than 10 times improvement on the electric field is demonstrated. **Figure 15** shows $\Delta\sigma$ and T_e as function of V_{GS} under V_{DS} of 0.1 and 10 V and both increases with the increased V_{DS}. The increase of $\Delta\sigma$ and T_e enhances PCF and POP scatterings at V_{DS} = 10 V, as shown in **Figure 16**. Therefore, a significant decrease of μ_G at V_{DS} = 10 V is demonstrated.

Conclusions

In summary, C_G extracted from high-frequency small-signal equipment circuit is used for the InAlN/GaN high electron mobility transistors (HEMTs) with sub-100 nm gate length. μ under V_{DS} of 0.1 V and 10 V are extracted with two-dimensional scattering theory, respectively. Under high electric field, the increased T_e and $\Delta\sigma$ enhances POP and PCF scatterings, resulting in the degradation of electron mobility, which hiding the improvement of the device performance of GaN HEMTs. Hence, in the further study, the method to improve electron mobility by decreasing $\Delta\sigma$ and T_e, should be very important for the application of GaN HEMTs.

Methods

Sample fabrication. Figure 1 shows the schematic of the fabricated InAlN/GaN HEMT on Si substrate. The epitaxial structures are grown with metalorganic chemical vapor deposition (MOCVD), which consists of a 2-μm undoped GaN buffer layer, a 4-nm $In_{0.12}Ga_{0.88}N$ back-barrier layer, a 15-nm GaN channel layer, a 1-nm AlN interlayer, an 8-nm lattice-matched $In_{0.17}Al_{0.83}N$ barrier layer, and a 2-nm GaN cap layer. Fabrication process started with device mesa isolation by using Cl_2-based inductively coupled plasma (ICP) etching. Source and drain ohmic contacts were formed with

Ti/Al/Ni/Au metal stack deposition and annealing at 850˚C for 40s. Finally, T-shaped gate was fabricated with electron beam lithography and Ni/Au deposition. Devices with source-drain distance (L_{SD}) of 2 μm, gate length (L_G) of 60 ~ 150 nm, and gate width (W_g) of 20 × 2 μm were fabricated.

Measurements. Current-voltage (I−V) measurements for the InAlN/GaN HEMTs were performed at room temperature using an Agilent B1500A semiconductor parameter analyzer, and capacitance-voltage (C−V) measurements were performed at room temperature using an Agilent B1520A at 1MHz. The S-parameters are taken with Anritsu MS4647B vector network analyzer configured to operate from 1 to 65 GHz.

Acknowledgments

This work was supported in part by the NASA International Space Station under Grant 80NSSC20M0142, and in part by Air Force Office of Scientific Research under Grant FA9550-19-1-0297 and Grant FA9550-21-1-0076.

Author contributions

P. C. and Y. Z. contributed to the research design, experiment measurements, data analysis, and manuscript preparation. All authors reviewed this manuscript.

Additional information

Competing financial interests: The authors declare no competing interests.

References

1 Tang, Y. *et al.* Ultrahigh-Speed GaN High-Electron-Mobility Transistors With f_T/f_{max} of 454/444 GHz. *IEEE Electron Device Lett.* **36**, 549-551 (2015).

2 Then, H. W. *et al.* Gallium Nitride and Silicon Transistors on 300 mm Silicon Wafers Enabled by 3-D Monolithic Heterogeneous Integration. *IEEE Trans. Electron Devices* **67**, 5306-5314, doi:10.1109/TED.2020.3034076 (2020).

3 Marti, D. *et al.* 94-GHz Large-Signal Operation of AlInN/GaN High-Electron-Mobility Transistors on Silicon With Regrown Ohmic Contacts. *IEEE Electron Device Lett.* **36**, 17-19, doi:10.1109/Led.2014.2367093 (2015).

4 Schuette, M. L. *et al.* Gate-recessed integrated E/D GaN HEMT technology with f_T/f_{max}>300GHz. *IEEE Electron Device Lett.* **34**, 741-743, doi:10.1109/LED.2013.2257657 (2013).

5 Downey, B. P. *et al.* SiNx/InAlN/AlN/GaN MIS-HEMTs With 10.8 THz · V Johnson Figure of Merit. *IEEE Electron Device Lett.* **35**, 527-529, doi:10.1109/LED.2014.2313023 (2014).

6 Pengelly, R. S., Wood, S. M., Milligan, J. W., Sheppard, S. T. & Pribble, W. L. A review of GaN on SiC high electron-mobility power transistors and MMICs. *IEEE Trans. Microwave Theory Tech.* **60**, 1764-1783, doi:10.1109/TMTT.2012.2187535 (2012).

7 Marso, M. *et al.* Origin of improved RF performance of AlGaN/GaN MOSHFETs compared to HFETs. *IEEE Trans. Electron Devices* **53**, 1517-1523, doi:10.1109/TED.2006.875819 (2006).

8 Liu, Z. *et al.* Improved two-dimensional electron gas transport characteristics in AlGaN/GaN metal-insulator-semiconductor high electron mobility transistor with atomic layer-deposited Al_2O_3 as gate insulator. *Appl. Phys. Lett.* **95**, 223501, doi: https://doi.org/10.1063/1.3268474 (2009).

9 Dai, S. *et al.* High f_T AlGa (In) N/GaN HEMTs Grown on Si With a Low Gate Leakage and a High ON/OFF Current Ratio. *IEEE Electron Device Lett.* **39**, 576-579, doi:10.1109/LED.2018.2809689 (2018).

10 Gurusinghe, M., Davidsson, S. & Andersson, T. Two-dimensional electron mobility limitation mechanisms in $Al_xGa_{1-x}N$/GaN heterostructures. *Phys. Rev. B* **72**, 045316, doi:https://doi.org/10.1103/PhysRevB.72.045316 (2005).

11 Polyakov, V. *et al.* Intrinsically limited mobility of the two-dimensional electron gas in gated AlGaN/GaN and AlGaN/AlN/GaN heterostructures. *J. Appl. Phys.* **106**, 023715, doi:https://doi.org/10.1063/1.3174441 (2009).

12 Cui, P. *et al.* Influence of different gate biases and gate lengths on parasitic source access resistance in AlGaN/GaN heterostructure FETs. *IEEE Trans. Electron Devices* **64**, 1038-1044, doi:10.1109/TED.2017.2654262 (2017).

13 Dang, X. *et al.* Measurement of drift mobility in AlGaN/GaN heterostructure field-effect transistor. *Appl. Phys. Lett.* **74**, 3890-3892, doi:https://doi.org/10.1063/1.124214 (1999).

14 Fang, T., Wang, R., Xing, H., Rajan, S. & Jena, D. Effect of optical phonon scattering on the performance of GaN transistors. *IEEE Electron Device Lett.* **33**, 709-711, doi:10.1109/LED.2012.2187169 (2012).

15 Cui, P. *et al.* Effect of Different Gate Lengths on Polarization Coulomb Field Scattering Potential in AlGaN/GaN Heterostructure Field-Effect Transistors. *Sci. Rep.* **8**, 9036, doi:https://doi.org/10.1038/s41598-018-27357-6 (2018).

16 Yang, M. *et al.* Effect of polarization Coulomb field scattering on parasitic source access resistance and extrinsic transconductance in AlGaN/GaN heterostructure FETs. *IEEE Trans. Electron Devices* **63**, 1471-1477, doi:10.1109/TED.2016.2532919 (2016).

17 Kordoš, P., Gregušová, D., Stoklas, R., Čičo, K. & Novák, J. Improved transport properties of Al_2O_3 / Al Ga N / Ga N metal-oxide-semiconductor heterostructure field-effect transistor. *Appl. Phys. Lett.* **90**, 123513, doi:https://doi.org/10.1063/1.2716846 (2007).

18 Koomen, J. Investigation of the MOST channel conductance in weak inversion. *Solid-State Electron.* **16**, 801-810, doi:https://doi.org/10.1016/0038-1101(73)90177-9 (1973).

19 Kim, D.-H., Brar, B. & Del Alamo, J. A. in *2011 International Electron Devices Meeting*. 13.16. 11-13.16. 14 (IEEE).

20 Romanczyk, B. *et al.* Bias-Dependent Electron Velocity Extracted From N-Polar GaN Deep Recess HEMTs. *IEEE Trans. Electron Devices* **67**, 1542-1546, doi:10.1109/TED.2020.2973081 (2020).

21 Kim, D.-H., Del Alamo, J., Antoniadis, D. & Brar, B. in *2009 IEEE International Electron Devices Meeting (IEDM).* 1-4 (IEEE).

22 Bouzid-Driad, S. *et al.* AlGaN/GaN HEMTs on Silicon Substrate With 206-GHz f_{max}. *IEEE Electron Device Lett.* **34**, 36-38, doi:10.1109/LED.2012.2224313 (2012).

23 Crupi, G. *et al.* Accurate multibias equivalent-circuit extraction for GaN HEMTs. *IEEE Trans. Microwave Theory Tech.* **54**, 3616-3622, doi:10.1109/TMTT.2006.882403 (2006).

24 Lv, Y. *et al.* Polarization Coulomb field scattering in AlGaN/AlN/GaN heterostructure field-effect transistors. *Appl. Phys. Lett.* **98**, 123512, doi:https://doi.org/10.1063/1.3569138 (2011).

25 Luan, C. *et al.* Theoretical model of the polarization Coulomb field scattering in strained AlGaN/AlN/GaN heterostructure field-effect transistors. *J. Appl. Phys.* **116**, 044507, doi:https://doi.org/10.1063/1.4891258 (2014).

26 Anwar, A., Webster, R. T. & Smith, K. V. Bias induced strain in AlGaN/GaN heterojunction field effect transistors and its implications. *Appl. Phys. Lett.* **88**, 203510, doi:https://doi.org/10.1063/1.2203739 (2006).

27 Matulionis, A. *et al.* Hot-phonon temperature and lifetime in a biased Al x Ga 1− x N/G a N channel estimated from noise analysis. *Phys. Rev. B* **68**, 035338, doi:https://doi.org/10.1103/PhysRevB.68.035338 (2003).

28 Yang, M. *et al.* Study of gate width influence on extrinsic transconductance in AlGaN/GaN heterostructure field-effect transistors with polarization Coulomb field scattering. *IEEE Trans. Electron Devices* **63**, 3908-3913, doi:10.1109/TED.2016.2597156 (2016).